Inorganic Chemistry

Nanoblock Coupling Effect in Iodine Intercalated [Bi$_{0.82}$CaO$_2$]$_2$[CoO$_2$]$_{1.69}$ Layered Cobaltite

E. Guilmeau,*,[†,‡,§] M. Pollet,[∥] D. Grebille,[†] M. Hervieu,[†] H. Muguerra,[†] R. Cloots,[§] M. Mikami,[‡] and R. Funahashi[‡]

CRISMAT-ENSICAEN Laboratory, UMR CNRS 6508, 6 Bd. Maréchal Juin, 14050 Caen Cedex, France, National Institute of Advanced Industrial Science and Technology, Midorigaoka, Ikeda, Osaka 563-8577, Japan, Laboratory of Structural Inorganic Chemistry, University of Liège, Chemistry Department B6, Sart-Tilman B4000 Liège, Belgium, and Institut de Chimie de la Matière Condensée de Bordeaux (ICMCB)—CNRS, Université de Bordeaux 1, 87 Avenue du Dr A. Schweitzer, F-33608 PESSAC, France.

We report on the structural, microstructural, and electronic properties of iodine intercalated [Bi$_{0.82}$CaO$_2$]$_2$[CoO$_2$]$_{1.69}$ misfit cobaltite. We first prove through a detailed and careful structural study that the block layer structure can be modified in the desired way. Iodine enters the material between the [BiO] double layers, and the *c*-cell parameter of the pristine compound is elongated by 3.6 Å. On the basis of this result, we point out the coupling between the block-layer structure and the transport properties. Additionally, we provide in-depth commentary and discussion of some extra results, clarifying some doping effects in the quasi-2D studied phase. Finally, we also propose some expressions that might be useful to material scientists for the tuning of the properties of such compounds.

I. Introduction

At the beginning of the 1990s, interest within the material science community for high-T_c bismuth cuprates led several researchers to successfully investigate the intercalation.[1–3] The block-layer structure of these oxides was shown to be easily intercalated between the weakly coupled [BiO] double layers, leading to a significant expansion of the lattice along the *c*-axis. For the study of the mechanisms responsible for high-T_c superconductivity, structural modification was given serious consideration in these materials, with a view toward engineering their properties and synthesizing other promising high-T_c superconductors.

Among the transition metal oxides studied in the two last decades, the layered cobaltites, Na$_x$CoO$_2$,[4] Ca$_3$Co$_4$O$_9$,[5–7] and Bi$_2$Sr$_2$Co$_2$O$_x$,[8] have opened the way for the exploration of new thermoelectric materials and for the development of polycrystalline bulk materials with potential applications. Thermoelectric generation systems can convert heat energy into electrical energy without using any moving part such as turbines and without producing any detrimental emissions such as carbon dioxide gas or radioactive substances. To realize thermoelectric power generation, a thermoelectric figure of merit higher than 1.0 is required (ZT = $S^2 T/\rho\kappa$; S, Seebeck coefficient; T, temperature; ρ, electric resistivity; and κ, thermal conductivity) but also a high chemical stability and no harmful elemental content. For this purpose, oxide materials are among the strongest candidates, and more particularly, the layered CoO$_2$-based single crystals, Ca$_3$-Co$_4$O$_9$, with a p-type behavior have a sufficiently high thermoelectric figure of merit (ZT) at high air temperature to focus research interest.[7]

Because of their structural similarity with bismuth cuprates, layered Bi/(Ca,Sr)/Co/O cobaltites are interesting candidates

* To whom correspondence should be addressed. E-mail: emmanuel.guilmeau@ensicaen.fr.
† CRISMAT-ENSICAEN Laboratory.
‡ National Institute of Advanced Industrial Science and Technology.
§ Laboratory of Structural Inorganic Chemistry.
∥ Institut de Chimie de la Matière Condensée de Bordeaux.

(1) Xiang, X.-D.; McKernan, S.; Vareka, W. A.; Zettl, A.; Corkill, J. L.; Barbee, T. W.; Cohen, M. L. *Nature* **1990**, *348*, 145.
(2) Xiang, X. D.; Vareka, W. A.; Zettl, A.; Corkill, J. L.; Cohen, N. Kijima, M. L.; Gronsky, R. *Phys. Rev. Lett.* **1992**, *68*, 530.
(3) Subramanian, M. A. *J. Solid State Chem.* **1994**, *110*, 193.
(4) Terasaki, I.; Sasago, Y.; Uchinokura, K. *Phys. Rev. B: Condens. Matter* **1997**, *56*, R12685.
(5) Li, S.; Funahashi, R.; Matsubara, I.; Ueno, K.; Yamada, H. *J. Mater. Chem.* **1999**, *9*, 1659.
(6) Masset, A. C.; Michel, C.; Maignan, A.; Hervieu, M.; Toulemende, O.; Studer, F.; Raveau, B.; Hejtmanek, J. *Phys. Rev. B: Condens. Matter* **2000**, *62*, 166.
(7) Shikano, M.; Funahashi, R. *Appl. Phys. Lett.* **2003**, *82*, 1851.
(8) Funahashi, R.; Matsubara, I.; Sodeoka, S. *Appl. Phys. Lett.* **2000**, *76*, 2385.

for intercalation. Their structure consists of an alternating hexagonal CoO_2 layer and a quadruple rock-salt layer composed of a double [Bi−O] layer. Intercalation chemically modifies the block-layer structure, allowing the control of physical properties. It also offers an alternative path to significantly improve our understanding of the system through the investigation of the mechanisms responsible for the high ZT values. We report here the successful synthesis and preliminary physical characterization of iodine intercalated $[Bi_{0.82}CaO_2]_2[CoO_2]_{1.69}$ single crystals.

II. Experiment

Single crystals (SC) of pristine Bi−Ca−Co−O were grown by the flux method. Precursor powders of Bi_2O_3, $CaCO_3$, and Co_3O_4 were mixed with a cationic composition of Bi/Ca/Co = 2.5/2.5/2 and calcined at 850 °C for 50 h. The resulting powder was mixed and calcined again in the same conditions. The powder was then mixed with Bi_2O_3 powder (weight ratio of 1/0.5) and heated in an alumina crucible at 1050 °C for 20 h. The temperature was cooled to 700 °C at a rate of 2 °C/h and was then furnace-cooled.

Iodine intercalation was achieved by vacuum-sealing the SC specimens with excess elemental iodine in a glass tube. Intercalation was carried out at 120 °C for 50 h. The pristine composition and the amount of iodine introduction into the host material were both determined by energy and wavelength dispersive spectroscopy (EDS and WDS) analysis. Several crystals were analyzed each time, and their compositions were found to be homogeneous. The calcium site is taken as a reference and set to 2 in the following. This choice is validated by the structural analysis (see section III). With the use of EDS, the average composition is found to be $Bi_{1.73}Ca_2Co_{1.47}$-$Al_{0.28}O_x$. With the use of WDS, the composition was averaged for more than 800 measurements on several crystals, and they were shown to have a very weak cationic ratio dispersion of $Bi_{1.65(3)}$-$Ca_{2.00(4)}Co_{1.47(4)}Al_{0.22(2)}O_x$. This composition, with its uncertainties, matches with the one resulting from the structural analysis. The cationic ratios are the same for the intercalated compound, and a 0.98/2 ratio of I to Ca is found. For all these materials, the aluminum was supplied by the crucible.

Two types of single-crystal X-ray diffraction experiments were performed: (i) large (00l) oriented crystals (3 mm × 3 mm) were used for $2\theta-\omega$ scans using a two-circle diffractometer (Rigaku RINT-TTR) with Cu Kα radiation, and (ii) small single-crystal samples were selected from the preparations for a global data collection using a four-circle Bruker KappaCCD diffractometer with Mo Kα radiation. Crystals were systematically characterized by a very large mosaicity that did not allow performing a global data reduction for the complete structure refinement; however, their crystalline quality was sufficient for a first description of the crystal symmetry by synthetic precession images.

The sample for transmission electron microscopy was prepared by fine crushing of one of the single crystals in alcohol, and the small flakes in suspension were deposited onto a porous carbon film, supported by a copper grid. The electron diffraction (ED) study was carried out at room temperature with a JEOL 200CX electron microscope, and the high-resolution electron microscopy (HREM) was performed with a Topcon 002B microscope (V = 200 kV, Cs = 0.4 mm).

The Seebeck coefficient (S) was measured in a range from 90 to 340 K using a MMR Technologies, Inc., measurement system. Electrical resistivity (ρ) measurements were performed at 25−300 K using a dc four-probes method.
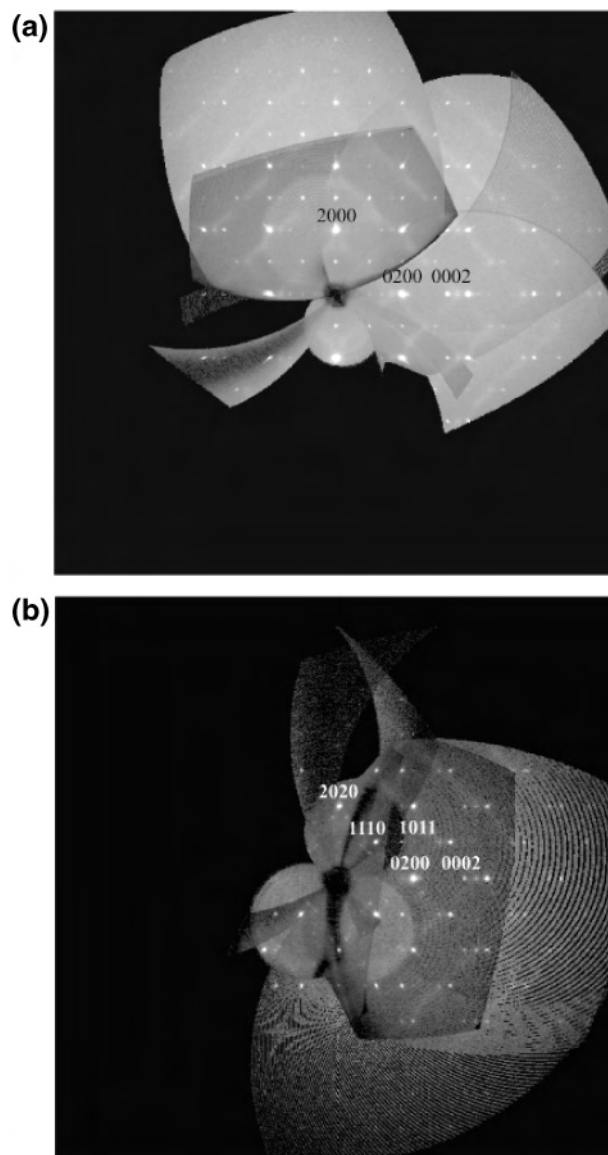
Figure 1. ($hk0$) Synthetic precession image (a) of the $[Bi_{0.82}CaO_2]_2$-$[CoO_2]_{1.69}$ compound and (b) of the $I[Bi_{0.82}CaO_2]_2[CoO_2]_{1.69}$ compound. The indexation is given with the *H,K,L,M* quadruplet compatible with the superspace symmetry $P2/m$ (0δ1/2) in (a) and $A2/m$ (0δ1) in (b).

The magnetic measurements were carried out over a 2−320 K range using a Quantum Design MPMS facility equipped with a SQUID magnetometer. Several single crystals were stacked (typically 20 SC). The M(H) curves at 4 K are characteristic for paramagnets (not shown). A magnetic field of 4 T was applied parallel to the (ab) planes for the M(T) measurements. The total susceptibility was fitted using the expression $\chi(T) = \chi_{dia} + \chi_{vv} + \chi_{cw}(T)$, with χ_{dia} being the core electrons diamagnetism, χ_{vv} as the VanVleck independent paramagnetic contribution, and χ_{cw} describing the standard Curie−Weiss dependence.

III. Structural Analysis

A. **Crystal Symmetry of the Nonintercalated Crystals (I_2 Free).** The synthetic precession images agree with the misfit character of the structure. Figure 1a clearly shows the two sublattices with their different b parameters: a = 4.90 Å b_1 = 4.73 Å, b_2 =2.80 Å, c = 14.66 Å, and β = 93.49°. As previously mentioned, a large mosaicity is also observed,

Table 1. Chemical Composition, Space Group, and Lattice Constants of Pristine and Intercalated Compound

	composition						lattice parameters				
compound	Bi	Ca	Co	Al	I	space group	a (Å)	b_1 (Å)	b_2 (Å)	c (Å)	β (deg)
pristine	2	1.99	1.44	0.28	∅	$P2/m$ $(0\delta 1/2)$	4.901	4.730	2.8	14.661	93.49
iodine intercalated	2	2.04	1.45	0.27	0.98	$A2/m$ $(0\delta 1)$	4.903	4.742	2.8	36.51	87.30

mainly in the misfit b direction. The ($hk0$) plane looks very similar to the corresponding plane of the related Sr misfit[9] compound $[Bi_{0.87}SrO_2]_2[CoO_2]_{1.82}$. The slightly different ratio ($\delta = b_1/b_2 = 1.69$) calculated here simply illustrates the shortening of the b_1 parameter of the [BiCaO₂] sublattice due to the replacement of Sr^{2+} by the smaller Ca^{2+} cation. The synthetic formulation for our crystals is given as $[Bi_{0.87}CaO_2]_2[CoO_2]_{1.69}$. A small amount of aluminum was also detected in the SC but is not considered in this part of the discussion. The main difference with the Sr compound is that the first sublattice is only compatible with a primitive cell, even if a rough C pseudosymmetry is observed; the reflections related to the second sublattice are only compatible with a double c parameter and an A centered lattice. In the framework of the superspace symmetry for aperiodic structures,[10] the corresponding superspace Laue class is $P2/m$ $(0\delta^1/_2)$.

Crystal Symmetry of Iodine Intercalated Crystals. Similar data collections were performed with intercalated I_2 crystals. Very similar results were obtained concerning the precession images and the crystal symmetry. The only difference is the upper value for the c_1 parameter (18.305 instead of 14.66 Å). The aperiodic scheme of the intercalated structure is equivalent, and one can suppose that only the stacking scheme of the different layers is modified; this point will be discussed in the next section. Finally, a still larger mosaicity is now observed, probably related to the enhanced stacking disorders and misorientations in these very flexible lamellar samples.

Nevertheless, a more detailed analysis of the diffraction pattern reveals some significant differences (compare Figure 1b with Figure 1a) and anomalies using the previous monoclinic cell ($a_1 = 4.903$ Å, $b_1 = 4.742$ Å, $b_2 = 2.80$ Å, $c_1 = 18.305$ Å, and $\beta = 94.99°$). A new superspace symmetry analysis was performed and concluded with a new centered monoclinic lattice ($a'_1 = 4.903$ Å, $b'_1 = 4.742$ Å, $c'_1 = 36.51$ Å, and $\beta' = 87.30°$) and the Laue class of $A2/m$ $(0\delta 1)$. This point will be discussed elsewhere.[11]

C. Partial Structure Refinement of the Nonintercalated and Intercalated Compounds. A first step for a structural description is to give the proper stacking scheme along the c direction of the different layers of these lamellar compounds. A more accurate general structural refinement needs a more complicated analysis involving the aperiodic misfit character and also requires more reliable X-ray diffraction data collection with higher quality crystal samples.

Table 2. Refined z Atomic Positions from the Four-Circle Diffractometer Experiment Data Collection

	$[BiCaO_2]_2[CoO_2]_{1.69}$	$I[BiCaO_2]_2[CoO_2]_{1.69}$
Co	0	0
O1	0.070(1)	0.055 (2)
Ca	0.1963 (4)	0.1613 (7)
O2	0.242 (3)	0.194 (5)
Bi	0.3842 (2)	0.3106 (3)
O3	0.370 (4)	0.282 (10)
I		0.5

In the following, we will only focus on the projection of the structure on the c-axis, using only the [00l] section of the reciprocal space.

A first refinement was performed using the (00l) ($5 \leq l \leq 25$) reflections of the four-circle diffractometer data collection. Only the z atomic coordinates and isotropic Debye−Waller parameters were refined, with a preliminary model deduced from the previously refined $[Bi_{0.87}SrO_2]_2[CoO_2]_{1.82}$ structure. A sufficiently good agreement factor ($R = 0.0254$, $R_w = 0.0295$) was obtained with the final z atomic positions listed in Table 2, to confirm the model. These final results were also used for a profile-fitting refinement of the two-circle data collection experiment. The agreement is also very good, as shown in Figure 2 ($R = 0.0439$, $R_w = 0.0294$, $R_p = 0.0585$, $R_{wp} = 0.0852$).

This first study clearly shows that the present $[Bi_{0.82}CaO_2]_2[CoO_2]_{1.69}$ structure is isotypic with the $[Bi_{0.87}SrO_2]_2[CoO_2]_{1.82}$ one, as far as the average structure is concerned and taking into account the steric modification related to the atomic radius of Sr and Ca. But a more detailed study is needed for the accurate description of the involved incommensurate modulations.

Now, it is interesting to consider the I_2 intercalated sample to confirm the localization of I between the [BiO] double layers.[12] A new model was built using the previous BiO−CaO−CoO₂−CaO−BiO stacking model and by adding an iodine layer at $z = 0.5$. The model was then refined using only the z coordinates, isotropic Debye-Waller parameters, and the site occupancy of the I site. A very good agreement was still obtained with the two experimental setups (Figure 2 and Table 2) ($R = 0.0276$, $R_w = 0.0295$ for the four-circle diffractometer experiment and $R = 0.0253$, $R_w = 0.0175$, $R_p = 0.0707$, and $R_{wp} = 0.111$ for the two-circle diffractometer experiment). The structural model is well confirmed with an average BiO−BiO distance which increases from 3.40 to 6.87 Å. The calculated Bi/Ca/I ratio (1.9/2.0/0.96) stands for an I occupation corresponding to one I atom for two Bi or Ca atoms.

According to the structural analysis, the c-axis cell parameter is modified from 14.6 to 18.2 Å by I_2 intercalation,

(9) Leligny, H.; Grebille, D.; Perez, O.; Masset, A. C.; Hervieu, M.; Raveau, B. *Acta Crystallogr., Sect. B* **2000**, *B56*, 173.

(10) Janssen, T.; Janner, A.; Looijenga, A.; de Wolff, P. M. *International Tables for Crystallography*; Wilson, A. J., Ed.; Kluwer Academic: Dordrecht, The Netherlands, 1992; Vol C, p 797.

(11) Grebille, D.; Muguerra, H.; Pérez, O.; Guilmeau, E.; Rousselière, H.; Funahashi, R. Submitted to *Acta Crystallogr. B*
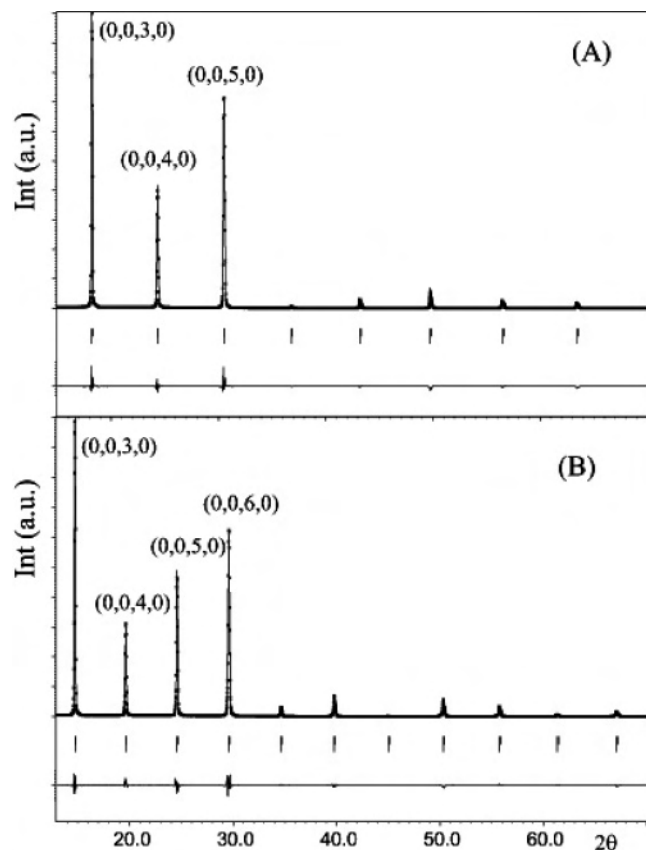
Figure 2. Refined X-ray diffraction pattern of (A) $[Bi_{0.82}CaO_2]_2[CoO_2]_{1.69}$ and (B) $I[Bi_{0.82}CaO_2]_2[CoO_2]_{1.69}$; crosses, experimental points; solid line, calculated profile. The difference curve is given below, with ticks corresponding to the diffraction lines. The proposed indexation is compatible with the $c_1 = c_2/2$ parameter.

which means that each intercalated iodine layer expands the c-axis by 3.6 Å (3.47 Å between the two [BiO] layers). This is consistent with the recent study on $Bi_2(Sr,Ca)_2Co_2O_x$ iodine intercalated whiskers[12] and previous reports on iodine intercalation in $Bi_2Sr_2CaCu_2O_8$ phase where an expansion of the c-axis unit cell dimension of 3.6 Å was observed.[1−3]

IV. Transmission Electron Microscopy

The electron diffraction study confirmed that the intense reflections of most of the analyzed crystallites involve a monoclinic cell, whose parameters are in agreement with those of the single-crystal picked up for the X-ray study, namely, $a_1 = 4.903$ Å, $b_1 = 4.742$ Å, $b_2 = 2.80$ Å, $c_1 = 18.305$ Å, and $\beta = 94.99°$.

The misfit character of the sample is clearly visible in the [001] ED patterns with $b_2^*/b_1^* \approx 1.69$, as illustrated by the two sets of reflections indexed considering the two sublattices in Figure 3a. Except for the curved shape of the reflections, commonly observed in lamellar structures and associated with slight rotation of the sheets around their perpendicular axis (see also the X-ray patterns), the $hk0m$ reflections are intense, without any signature of diffuse phenomenon. In the enlargement of the [001] patterns, all of the $hk0$ reflections are observed (see the white arrows), whereas for the second subsystem the condition of reflection is $hm0 : h + m = 2n$. Note that the $hk0 : h + k = 2n + 1$
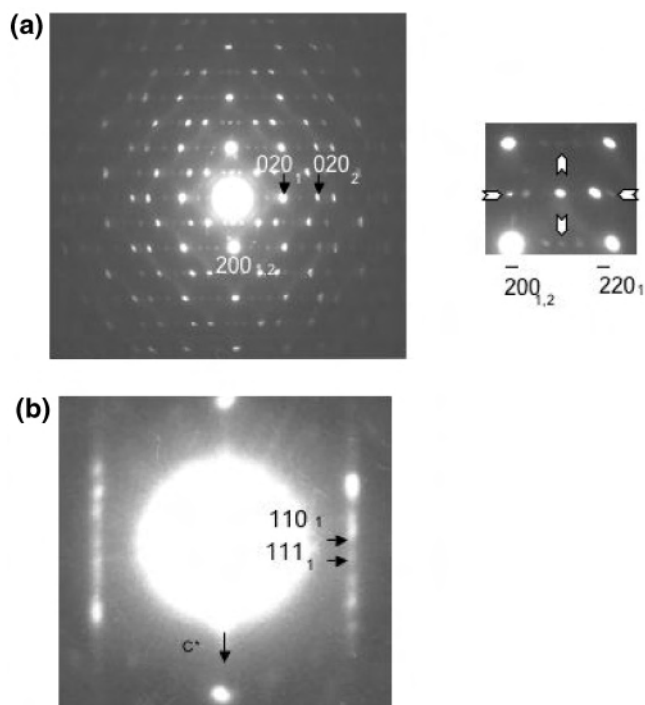

Figure 3. Iodine compound: (a) [001] ED pattern and enlargement showing the presence of $hk0$, $h + k = 2n + 1$ reflections; (b) $[\bar{1}10]_1$ ED pattern.
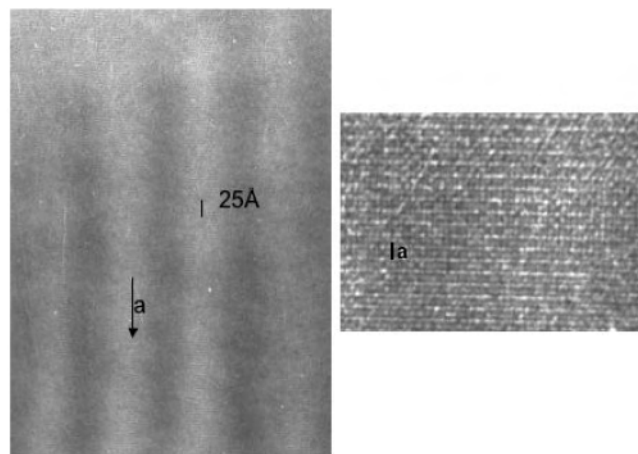

Figure 4. Overall and enlarged [001] high-resolution images.

reflections, which violate the C-centering of the first sublattice, are systematically present but characterized by a relative intensity varying with the selected flakes, from weak to scarcely visible.

In the [100] ED patterns, as along any [$0klm$] viewing direction, the sharpness of the reflections is considerably lower than along [001], and moreover, streaky lines along c^* are systematically present. This is exemplified in Figure 3b. The conditions of reflection are $0kl: k = 2n$ and $0ml: m + l = 2n$. Unfortunately, the diffuse phenomena prevent us from accurately reconstructing the reciprocal space.

The Moiré patterns (large bright and dark stripes) commonly observed in the [001] high-resolution images (Figure 4) are generated by the tiny disorientation of the sheets along the viewing direction. In the enlarged image, the 4.9 Å periodicity along $\vec{a}$ is clearly observed over the whole sheet,
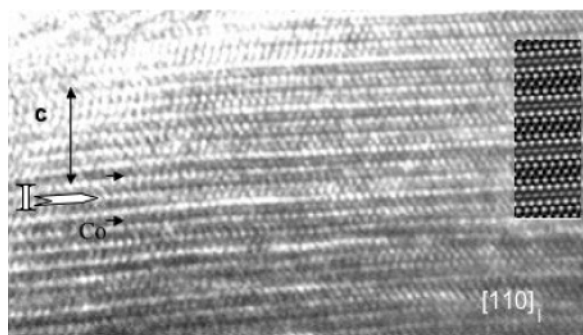
Figure 5. [001]₁ high-resolution image illustrating the stacking sequence of the different layers along $\vec{c}$.
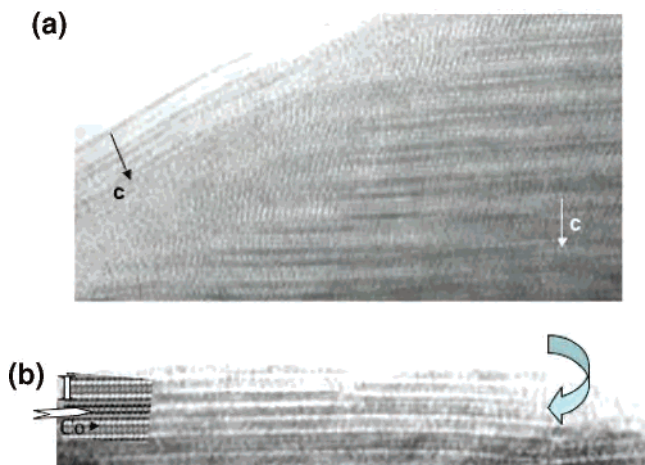

Figure 6. Typical examples of extended defects. (a) A double misfit sheet wraps the edge of a [001]₁ crystallite, and (b) interruption of the iodine layer in a [001] crystallite.

confirming that the presence of additional reflections (loss of the *C*-type symmetry of the first subcell) is not a local event.

The [100]₁ high-resolution image (Figure 5) allows confirmation of the stacking sequence of the layers along $\vec{c}$. The image has been recorded for a focus value close to −650 Å, where the high electron density zones are highlighted. The five layers building the rock-salt-related block are imaged as rows of staggered bright dots. They are separated by one row of less bright dots, associated with the Co layers. The simulated images have been calculated using the Mac Tempas software, on the basis of a theoretical model, which has been conceived by considering the $[Bi_2Ca_2O_4]\,[CoO_2]_{1.69}$ structure, X-ray data, and the experimental HREM images. The additional "I" layer, intercalated between two bismuth layers, appears rather disturbed—more so than the other layers. In fact, in a more general way, one often observes that the crystallinity is not perfect (by far), due to numerous extended defects. Two examples are given in Figure 6. In the [110]₁ high-resolution image of Figure 6a, the crystal edge is wrapped with a double misfit sheet, hugging the crystal shape (the $\vec{c}$ axis of the normal lamellar structure is shown by white lettering, whereas the $\vec{c}$ axis of the defective misfit is shown by black lettering). The second example presents a [100] HREM experimental and calculated image of the iodine sample in the left part of Figure 6b. In the
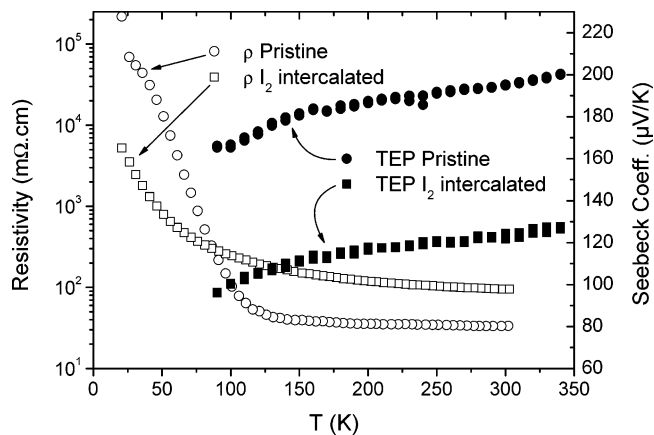
Figure 7. Temperature dependence of the electrical resistivity and thermopower for the pristine and the iodine intercalated compound. Key: (●) filled circles, TEP pristine; (■) filled squares, TEP I₂ intercalated; (○) empty circles, ln(σ) pristine; (□) empty-squares, ln(σ) I₂ intercalated.

right part, the iodine layer disappears, leading to the formation of a local $[Bi_2Ca_2O_4]\,[CoO_2]_{1.69}$ structure, the difference between the *c* parameters being quickly picked up. The HREM images show that such structural mechanisms often take place in the misfit structure and are easily accommodated by the different layers, which appear highly flexible. They also explain the streaky lines observed in the $[hk_1k_20]$ ED patterns.

V. Tranport Properties

Figure 7 shows the temperature dependence of the electrical resistivity and thermopower for pristine and iodine intercalated compounds. Intercalation drastically reduces the thermopower (TEP) over the entire temperature range. This result follows our expectation, since it is well-established that the intercalated iodine between the [BiO] double layers in superconducting bismuth cuprates induces a TEP decrease related to an increase of the hole concentration. In these Bi−cuprate systems, iodine is known to enter the material as linear triiodide (I_3^-) ions between the [BiO] layers,[13] and the TEP shifts toward lower values can be attributed to the hole-doping effect by charge transfer from the intercalated iodine layer to the CuO₂ plane. As a consequence, according to our structural analysis which illustrates the intercalation of iodine between the [BiO] double layers, we can expect a charge transfer between the intercalated rock-salt layer and the hexagonal CoO₂ layer, responsible for the transport properties.

The thermopower of both small polaronic systems and band semiconductors is governed by the thermal activation of carriers across a small barrier and is generally well described[14] by eq 1
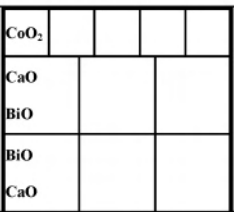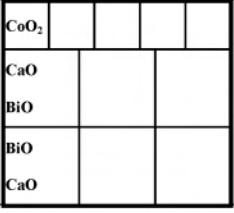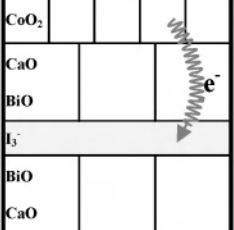
$$S = \frac{k_B}{e}\left(\frac{E_s}{k_B T} + b\right) \qquad (1)$$

Es being the carrier creation energy and *b* related to the

(12) Funahashi, R.; Guilmeau, E.; Maeda, Y.; Mikami, M.; Mihara, T. *Trans. Mater. Res. Soc. Jpn.* **2005**, *30*, 523.
(13) Kishio, K.; Pooke, D.; Trodahl, H. J.; Subramanian, C. K.; Kotaka, Y.; Seto, M.; Kitao, S.; Maeda, Y. *J. Supercond.* **1994**, *7*, 117.

Table 3. Thermoelectric and Magnetic Properties for All Investigated Samples

Material	Structure [1]	TEP∞, $r = Co^{III}/Co^{IV}$ [2,3]	Magnetization data [4]	Trend, ρ^{300K}, ρ^{∞}, $E\sigma$ [5]
CaBiCoO *	CoO₂ / CaO / BiO / BiO / CaO	$TEP^{300K} = 157.5\ \mu V/K$ $r = \dfrac{0.24}{0.76} = \dfrac{1-x}{x}$	$Co^{IV} = 0.24$ $\theta = -2\ K$	$\dfrac{d\rho}{dT} < 0$ up to 280K $\rho^{300K} = 16\ m\Omega.cm$
CaBiCoO SC Al³⁺ substituted This work	CoO₂ / CaO / BiO / BiO / CaO	$TEP^{\infty} = 240\ \mu V/K$ $r = \dfrac{0.11}{0.89}$	$C = 0.11\ ;\ C/Co = 0.07$ $Co^{IV} = 0.19\ ;\ \theta = -3\ K$	$\dfrac{d\rho}{dT} < 0$ $\rho^{300K} = 33\ m\Omega.cm$ $\rho^{\infty} = 28\ m\Omega.cm$ $E\sigma = 4.25\ meV$
Iodine-Intercalated CaBiCoO SC Al³⁺ substituted This work	CoO₂ / CaO / BiO / I₃⁻ (e⁻) / BiO / CaO	$TEP^{\infty} = 134\ \mu V/K$ $r = \dfrac{0.29}{0.71}$	$C = 0.18\ ;\ C/Co = 0.12$ $Co^{IV} = 0.32\ ;\ \theta = -8\ K$	$\dfrac{d\rho}{dT} < 0$ $\rho^{300K} = 95\ m\Omega.cm$ $\rho^{\infty} = 58\ m\Omega.cm$ $E\sigma = 12.54\ meV$

*Pollet et al., *J. Appl. Phys.*, in press. [1] Depicted using a $^5/_3$ misfit ratio (=1.69 from XRD data). [2] PTE∞ from S vs $1/T$ curves for ($1/T \rightarrow 0$). [3] R from the Heikes PTE formula for the high-temperature limit; assuming LS states for both Co^{III} and Co^{IV}. [4] Percent Co^{IV} from the Curie constant from χ^{-1} (T) curves; assuming LS states for both Co^{III} and Co^{IV}. [5] ρ^{∞}, $E\sigma$ from $\ln(\sigma)$ vs $1/T$ curves (limit for $1/T \rightarrow 0$ and $k_B \times$ slope).

Heikes modified factor relative to the degenerancy (g) and concentration of Co^{III} ($1 - x$) and Co^{IV} (x)

$$b = \ln\left(\frac{g^{IV}}{g^{III}}\frac{1-x}{x}\right) = \ln(\beta r) \qquad (2)$$

The first term in eq 1 gives the temperature dependence of the Seebeck coefficient; it applies to the carrier's activated systems, and one expects in this case a decrease of S with increasing T. The present experiments show an opposite behavior with an increase of the thermopower with T; this behavior is inherent to these lamellar cobaltites. However, until now, no definitive explanation could be drawn. Even though the observed temperature dependence contradicts eq 1, the high-temperature regime can be well-reproduced with a linear fit versus $1/T$ and a negative slope. The second term in eq 1 is developed in eq 2; the constant at the high-temperature term is shown to account for the carrier concentration, and as already suggested in our previous report dealing with the non-Al-substituted sample,[15] the spin-only degeneracy accounts for the observed electronic properties. S^{∞} (the thermopower in the high-temperature limit) and x, assuming Co^{III} and Co^{IV} in LS states and excluding any mixed valence for Bi, were calculated; the results, together with the data for an Al-free sample[15] are summarized in Table 3.

Let us first consider the enhancement of the thermopower from the Al-free sample to the present Al-substituted SC.

The high-temperature value of 140 $\mu V/K$, observed by Maignan et al.,[16] led to $x = 0.28\%$, and our results with a high-temperature limit of ~157 $\mu V/K$ led to $x = 0.24$. On the basis of the electroneutrality principle and given the average composition obtained in this last material ($Ca_2Bi_{1.62}Co_{1.62}O_{7.38-\delta}$), the global deficiency in oxygen should be $\delta = 0.32$. Several reports already state the deficiency of the CoO_2 layer in Na_xCoO_2,[17-19] and if the oxygen vacancies are here also located in the CoO_2 layers, the composition should be written as

$$[Ca_2Bi_{1.62}O_4][(Co_{0.24}{}^{4+}Co_{0.76}{}^{3+})_{(1.62/1.69)}\delta_{(0.07/1.69)}O_{2-0.19}]_{1.69}$$
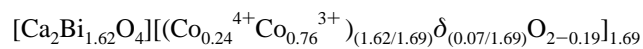
Using the results of Maignan et al. and assuming a 2+ valence for the cobalt in the rock-salt layer, one obtains an average $\delta = 0.25$, and in the CoO_2 layer, $\delta_{CoO_2} = 0.15$. These results are in reasonable agreement. Even if so high deficiency has already been observed in the CoO_2 layers;[17-19] these values are slightly high, and one should certainly assume that the vacancies here are more probably spread over both the CoO_2 layer and the weaker BiO ones. The preliminary XRD results are in favor of this last

(14) Salamon, M. B.; Jaime, M. *Rev. Mod. Phys.* **2001**, *73*, 583.

(15) Pollet, M.; Guilmeau, E.; Grebille, D.; Fagnard, J. F.; Cloots, R. *J. Appl. Phys.*, in press.
(16) Maignan, A.; Hébert, S.; Hervieu, M.; Michel, C.; Pelloquin, D.; Khomskii, D. *J. Phys.: Condens. Matter* **2003**, *15*, 2711.
(17) Bañobre-López, M.; Rivadulla, F.; Caudillo, R.; López-Quintela, M. A.; Rivas, J.; Goodenough, J. B. *Chem. Mater.* **2005**, *17*, 1965.
(18) Karppinen, M.; Asako, I.; Motohashi, T.; Yamauchi, H. *Phys. Rev. B* **2005**, *71*, 092105.
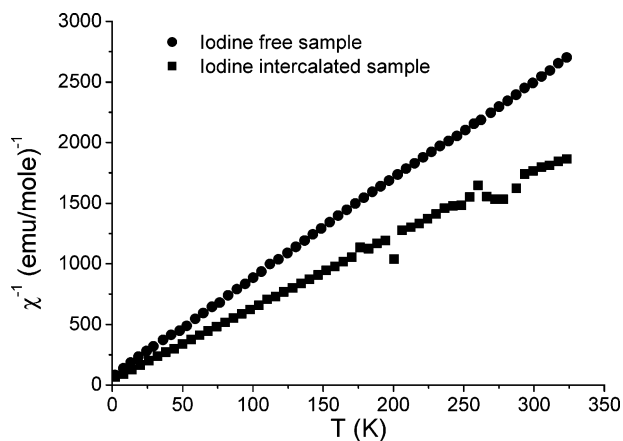
Figure 8. Inverse susceptibility vs T for the pristine and the iodine intercalated compounds (measurements with H // (ab) using ~20 stacked SC). Key: (●) filled circles, pristine; (■) filled squares, I_2 intercalated.
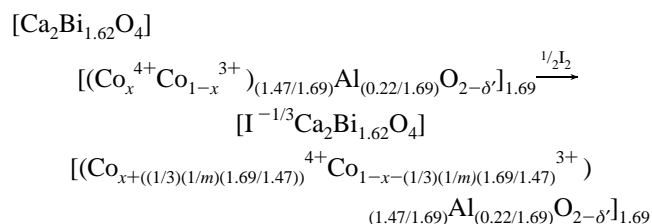
hypothesis, showing that the Bi−O layer contains some oxygen vacancies; however, the exact deficiency is still unknown. All of this remains purely speculative until accurate measurements of the oxygen content and the local cation environment are carried out to clarify this point. However, this missing information does not deserve the following argumentation.

Owing to both the primary structure analysis and the spectroscopic analysis, the aluminum substitutes for the cobalt in the CoO_2 layers. The composition can be written as

$$[Ca_2Bi_{1.62}O_4][(Co_x^{4+}Co_{1-x}^{3+})_{(1.47/1.69)}Al_{(0.22/1.69)}O_{2-\delta'}]_{1.69}$$
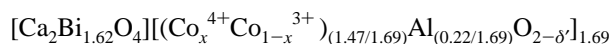
Assuming that the Al substitution should not interfere with the oxygen content and thus setting $\delta' = 0.19$, one can calculate the average Co valence as $v = 3.12$, i.e., a Co^{4+} concentration of $x = 0.12$ (Co^{IV} and Co^{III} in LS state). This value is in good agreement with the one obtained from the high-temperature limit of the Seebeck coefficient, $x = 0.11$ (Figure 7, Table 3). This Co^{IV} concentration is also in reasonable agreement with the one found from the magnetic measurements (Figure 8, Table 3).

The decrease of the thermopower upon intercalation can again simply be explained on the basis of structural considerations and the electroneutrality principle using the same argumentation. If one consider both the constant misfit ratio $m = 1.69$ for the structure and the -1 valence of an iodine triplet, I_3^- (each triplet able to oxidize one Co^{3+} to one Co^{4+}), and assuming that the intercalation does not change the oxygen content (intercalation in a sealed ampule), the reaction can be written as

$[Ca_2Bi_{1.62}O_4]$

$$[(Co_x^{4+}Co_{1-x}^{3+})_{(1.47/1.69)}Al_{(0.22/1.69)}O_{2-\delta'}]_{1.69} \xrightarrow{1/2 I_2}$$

$[I^{-1/3}Ca_2Bi_{1.62}O_4]$

$$[(Co_{x+((1/3)(1/m)(1.69/1.47))}^{4+}Co_{1-x-(1/3)(1/m)(1.69/1.47)}^{3+})$$
$$_{(1.47/1.69)}Al_{(0.22/1.69)}O_{2-\delta'}]_{1.69}$$

and the new calculated value for the Co^{IV} to Co^{III} ratio is

then $r = 0.35/0.65$. This value for the Co^{IV} content is slightly higher than the one obtained from the high-temperature limit of the Seebeck coefficient $x_I = 0.29$ (Figure 7, Table 3) (x_I = Co^{4+} concentration in I-intercalated compound); one should notice that this difference can easily be explained on the basis of the dependence of the former value on both the bismuth and the oxygen content and on the precision of the Seebeck data measurement for the last value. Note also that some iodine vacancies have been observed using the TEM (part IV) and that they can also account for this discrepancy, even though the intercalation is greatly facilitated by the weakness of the interaction between the two adjacent BiO layers.[9] The value for x_I calculated from the magnetic measurements (Figure 8, Table 3) is 0.32 and confirms the other measurements.

Concerning the electrical conductivity, let us first discuss the high electrical resistivity ($\rho_{300K} \sim 33$ mΩ·cm) measured on the SC pristine, in contrast to recent results published in the literature with values as low as $\rho = 16$ mΩ·cm measured on textured materials (in the ab planes).[20] A quite logical explanation for such a behavior originates in the presence of Al in the misfit structure and the decrease of the hole concentration in the CoO_2 layers. On the other hand, according to the study of Kobayashi et al.[21] on the browmillerite oxide $Ca_{2-y}La_yCo_{2-x}Al_xO_5$, the Al substitution in the Co sites of the CoO_2 square lattice acts as a scattering center (disorder) for electric conduction, although it stabilizes the browmillerite structure at ambient pressure. If we consider the substitution of Al in the Co sites of our materials (i.e., in the CoO_2 hexagonal layers), we can expect the same phenomenon and, as a consequence, the increase of ρ. Although the hole concentration is increased in the iodine-intercalated cobaltite, ρ increases from 33 mΩ·cm in the I-free compound to 95 mΩ·cm in the intercalated one (300 K). This phenomenon could be explained by the presence of stacking faults and disorder induced by the intercalation. Recently, Funahashi et al. have also shown that the iodine can easily be intercalated in Bi(Sr,Ca)CoO whiskers.[12] Their TEM observations evidenced that, despite an overall homogeneous intercalation between the [BiO] layers, some areas are drastically disordered by the intercalation as observed in the present study. The same transport property trends were observed in these compounds, i.e., a decrease of both the thermopower and the electrical conductivity upon intercalation. Because it is widely accepted that the TEP is much less sensitive to the grain boundaries or microstructure defects than the electrical resistivity, we strongly believe that the stacking faults are the origin of the electrical resistivity increase. Note, however, that due to the hole-doping effect, a significant decrease in ρ could be expected in these compounds if the iodine intercalation is better controlled.

Both materials exhibit a semiconducting-like behavior ($T > 140$ K for the I-free compound; whole range of temperature for the intercalated one). In the case of the I-free compound, $E\sigma \sim 4.25$ meV ($T > 140$ K). In the case of the

(19) Gupta, R.; Manthiram, A. J. *Solid State Chem.* **1996**, *121*, 483.
(20) Guilmeau, E.; Mikami, M.; Chateigner, D.; Funahashi, R. *J. Mater. Res.* **2005**, *20*, 1002.

intercalated compound, $E\sigma = 12.54$ meV (whole range of temperature). The higher value obtained for $E\sigma$ for the intercalated compound could originate from the presence of the stacking faults mentioned above.

Finally, in addition to the results already mentioned concerning the magnetization data, one can note that the fits to the Curie−Weiss law from the magnetic measurements data for both compounds led to slightly negative Weiss temperature (~ -7 and ~ -8 K, respectively, for the I-free and the intercalated material), indicating very low antiferromagnetic interactions. However, no anomaly characteristic for any ordering, neither a long nor a short range one, was evident from the M(T) or M(H) curves. The temperature-independent paramagnetism term χ_{vv} used to fit the data for both compounds is nearly equal to 250×10^{-6} emu/mol of Co, in agreement with the values expected from the localization of the electron on Co^{3+}.[22,23]

VI. Conclusion

This study reports the synthesis, structural characterizations, and transport property measurements of pristine and iodine-intercalated misfit $[Bi_{0.82}CaO_2]_2[CoO_2]_{1.69}$ single crystals. Accurate X-ray analyses provided evidence for a misfit structure in both materials with two sublattices characteristic of these layered cobaltites. Iodine was found to enter the material between the [BiO] double layers, and the c-cell parameter of the pristine crystal is elongated by 3.6 Å. Upon intercalation, the thermopower is shifted toward lower values due to a hole-doping effect by charge transfer from the intercalated iodine layer to the hexagonal CoO_2 layer. Even if the iodine intercalation in our compounds does not improve the thermoelectric performances, the placement of the intercalated iodine layer in the structure and the resulting change in transport properties allow us to expect improved materials by controlling the nanoblock layers of these cobaltites. The question of reducing the thermal conductivity and the influence of the two-dimensionality on the phonon scattering is now under consideration. An in-depth study is underway through the investigation of other intercalated compounds and the study of their electrical and thermal properties.

IC0616378

(21) Kobayashi, W.; Satake, A.; Terasaki, I. *Jpn. J. Appl. Phys.* **2002**, *41*, 3025.
(22) Blangero, M.; Decourt, R.; Carlier, D.; Ceder, G.; Pollet, M.; Doumerc, J. P.; Darriet, J.; Delmas, C. *Inorg. Chem.* **2005,** *44*, 9299.
(23) Mabbs, F. E.; Machin, D. J. *Magnetism and Transition Metal Complexes;* Chapman and Hall: London, 1973.